Dielectric properties of sputtered $SrTiO_3$ films

H.-M. Christen,* J. Mannhart, E.J. Williams, and Ch. Gerber
IBM Research Division, Zurich Research Laboratory, CH-8803 Rüschlikon, Switzerland
(Received 8 November 1993)

The dielectric properties of ⟨100⟩-oriented epitaxial $SrTiO_3$ films as used in high-T_c heterostructures have been studied as a function of temperature and applied electric field by using *in situ* grown heterostructures ($Mg/SrTiO_3/SrTiO_3$:Nb and $Au/YBa_2Cu_3O_{7-x}/SrTiO_3/SrTiO_3$:Nb). The dielectric behavior of these films is characterized by a rather low sample capacitance as compared to bulk single-crystal values and by occurrences of maxima in the capacitance-voltage and capacitance-temperature curves. The maximum attainable polarization was found to be 80 mC/m^2 at 4.2 K. Complementary measurements on single crystals of $SrTiO_3$ and $SrTiO_3$:Nb reveal that the behavior of these $SrTiO_3$ thin films can be understood from the bulk properties with additional strong charge trapping at the film-substrate interface.

I. INTRODUCTION

The maximum dielectric polarization that can be withstood by an insulating layer is a critical parameter limiting the performance of devices based on high-T_c superconductor heterostructures and the quality of capacitors in very large-scale integration (VLSI) memory cells. Owing to their high dielectric constant and breakdown strength, strontium titanate ($SrTiO_3$) and related perovskites are promising candidates for such applications. $SrTiO_3$ has received much attention due to its intriguing structural and dielectric properties.[1,2] In contrast to other materials in which comparable dielectric polarizations can be obtained, $SrTiO_3$ is not ferroelectric but remains paraelectric down to the lowest temperatures due to quantum fluctuations.[3] As epitaxial films of good quality can now be obtained, $SrTiO_3$ has become an increasingly encouraging material for various applications.

$SrTiO_3$ has a lattice mismatch of only 1–2 % with high-T_c superconductors such as $YBa_2Cu_3O_{7-x}$, and is compatible with film growth of these materials. For these reasons, $SrTiO_3$ films are used in high-T_c heterostructures such as field-effect samples[4–7] and superconducting quantum interference devices (SQUID's).[8]

Also of great technological interest are $SrTiO_3$ films grown on bare[9–11] and Pt-covered silicon,[11–13] as the combination of $SrTiO_3$'s high polarizability and resistivity with a standard semiconductor makes $SrTiO_3$ a suitable candidate for VLSI devices such as dynamic random access memories (DRAM's).

Fundamental changes of the structural, dielectric, and transport properties of $SrTiO_3$ can be induced by doping. The addition of calcium, for example, leads to low-temperature ferroelectric behavior,[14] whereas oxygen vacancies or doping with niobium result in superconductivity at subkelvin temperatures.[15,16] $SrTiO_3$ doped to the $\approx 0.1\%$ level with niobium or tungsten is a degenerate semiconductor. Because no carrier freeze-out is observed down to liquid helium temperatures, and because of the compatibility with high-T_c superconductor thin film growth, $SrTiO_3$:Nb crystals are used as substrates in superconductor-insulator-semiconductor[4,5,17] and in superconductor-semiconductor[18–20] heterostructures.

Despite these important applications, a rather incomplete qualitative description of the dielectric behavior of epitaxial $SrTiO_3$ films is found in the literature. Recently, a strong dependence of the dielectric constant on an electric field applied at room temperature has been reported.[21] A detailed study of the temperature dependence of the dielectric properties and a quantitative comparison with single-crystal values have not yet been published. Thus we have studied the dielectric properties of $SrTiO_3$ thin films sputtered onto single-crystal $SrTiO_3$:Nb substrates as shown in Fig. 1. Results are presented for the dielectric polarization P and the capacitance C as a function of a bias voltage V at 4.2 K, as well as for the temperature dependence of the dielectric constant ε of the films. The analysis of these results requires a quantitative description of the dielectric behavior of single-crystal $SrTiO_3$. Therefore, the $P(V)$ relation for single-crystal $SrTiO_3$ has been measured between 4.2 K and 300 K and will be presented below.

The structure of the paper is as follows: After a short description of the measurement setup (Sec. II) the behavior of single crystals of pure (Sec. III) and Nb-doped (Sec. IV) $SrTiO_3$ is analyzed and discussed. Then, in Sec. V, results of the experiments on sputtered films are

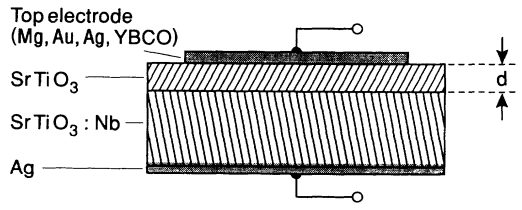

FIG. 1. Sample structure to study the dielectric properties of $SrTiO_3$ films. Mg, Au, Ag, and $YBa_2Cu_3O_{7-x}$, have been used as top electrode. The typical thickness d of the $SrTiO_3$ film is between 30 and 200 nm.

presented and compared to the behavior expected from the bulk properties.

II. MEASUREMENT SETUP

All samples used in this study were mounted on a temperature controlled sample holder with silver paint, yielding a temperature stability of better than ±100 mK. Measurements were performed in liquid helium or in helium gas.

For the polarization-voltage measurements, the voltage across the sample was swept by a Tektronix FG 504 function generator (sine wave or sawtooth shaped with frequencies ranging from 10^{-4} to 10^{-1} Hz and voltages up to 30 V peak to peak), while the sample current was recorded using a Keithley 642 electrometer. The polarization was obtained by numerical integration of this current.

The sample capacitance was analyzed with a Hewlett Packard HP4192A LF impedance analyzer (5 Hz–13 MHz). For *C-V* measurements, the bias was applied using an HP6634A System dc power supply, rather than using the impedance analyzer's built-in dc bias. This setup had the advantage that the current flowing through the sample was measured simultaneously with the capacitance, using a Keithley 195A multimeter, and that higher voltages (±100 V) could be applied. The dielectric response was measured with a test signal of typically 50 mV and 10 kHz superimposed to the bias voltage which was swept at a rate of about 0.5 V/min.

III. DIELECTRIC PROPERTIES OF SINGLE-CRYSTAL $SrTiO_3$

$SrTiO_3$ has a cubic perovskite structure at high temperatures and undergoes an antiferrodistortive transition at 108 K to a tetragonal state, this transition being unnoticeable in our dielectric measurements. Much rather, the $\varepsilon(T)$ behavior between room temperature and about 60 K can be described by a Curie law with a Curie temperature in the range of 30–36 K.[3,22] In the low-temperature, paraelectric phase, the dielectric constant saturates at a value of 24 000 (for ⟨100⟩-oriented samples).[3]

The maximum dielectric polarization $P_{\max}$ that can be induced in this material by the application of an electric field E is of particular technological interest, as $P_{\max}$ determines the maximum possible charge density stored in $SrTiO_3$-based devices. $P_{\max}$ is obtained as

$$P_{\max} = \int_0^{E_{BD}} \varepsilon_0[\varepsilon(E) - 1]\, dE, \tag{1}$$

where $\varepsilon_0 = 8.85\ \mathrm{pF\,m^{-1}}$. E_{BD} is the breakdown field and $\varepsilon(E)$ the small-signal dielectric constant at an applied bias field E. The values of E_{BD} and $\varepsilon(E)$ can be determined experimentally.

E_{BD} of single-crystal $SrTiO_3$ has been measured by Barret.[23] At 4.2 K, $E_{BD} = 4 \times 10^7$ V/m is found for samples with thicknesses ranging from 0.25 to 0.5 mm.

The field dependence $\varepsilon(E)$ has been studied[24–26] and analyzed in the framework of the Devonshire theory, where the contribution to the free energy arising from the electric polarization P is expanded in powers of P:

$$F = c_1(T)\, P^2 + c_2(T)\, P^4 + \cdots - EP. \tag{2}$$

At thermodynamic equilibrium ($\partial F/\partial P = 0$), this yields

$$E = \alpha(T)P + \beta(T)P^3 + \cdots \tag{3}$$

and the dielectric constant is obtained as

$$\varepsilon(E) = 1 + \frac{1}{\varepsilon_0}\frac{\partial P}{\partial E}. \tag{4}$$

(This notation differs from the one frequently used for semiconductors and optical devices,[27,28] where P is expanded in powers of E.)

In the above-mentioned studies,[24–26] a maximum of the $\varepsilon(T)$ curves of electric-field-biased single crystals at nonzero temperatures is reported. The decrease of ε as a consequence of the applied field was observed at all temperatures between 4.2 and 300 K, but it was strongest at the lowest temperatures. A later study[22] reports a field dependence of ε only below 65 K.

In order to check this dependence and to find the numerical values of the relevant parameters, we performed measurements on single-crystal $SrTiO_3$ samples.

Samples with a thickness ranging from 50 μm to 1 mm and a surface of a few square millimeters were cut along ⟨100⟩ directions from crystals supplied by Commercial Crystals, and polished with diamond paste (grain size of 1 μm) on a soft plastic film (3M IR1940). Au/Cr electrodes were evaporated after the samples had been cleaned with acetone in an ultrasonic bath, rinsed with isopropyl alcohol, and blown dry with nitrogen gas. Their low-field dielectric constant $\varepsilon(E \to 0)$ was deduced from measurements of the sample capacitance using

$$C = \varepsilon_0 \varepsilon \frac{A}{d},$$

where A is the sample surface and d its thickness. For a thin sample ($d = 57$ μm), the value ε=15 000 obtained at 4.2 K was considerably lower than the reported value of 24 000,[14] whereas no such strong deviation was found for thicker samples. The expected behavior was restored if the thin samples were etched, prior to electrode deposition, using the following procedure: the crystal was first immersed for 10 min in hot (100 °C) H_3PO_4 (85%), then in concentrated HCl (25 °C) to remove phosphates, and finally rinsed in boiling distilled water.

With this sample preparation, the value of ε as deduced from the capacitance was independent of thickness down to the thinnest of the etched samples investigated (d = 62 μm). Figure 2 shows $\varepsilon(E)$ for this specimen. Also shown in this figure are $\varepsilon(E)$ curves calculated according to Eq. (4), fitted by an adjustment of the free parameters $\alpha(T)$ and $\beta(T)$, and neglecting all terms of fifth or higher order in P [Eq. (3)]. These fit parameters, describing the dielectric polarizability over the entire field-temperature range investigated, are presented in Fig. 3.

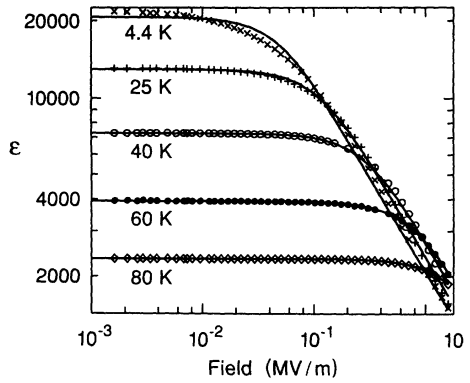

FIG. 2. Field dependence of the dielectric constant ε of single-crystal $SrTiO_3$ at various temperatures. Solid lines are fits to Eqs. (3) and (4).

Figure 4 shows the dielectric constant as derived from the parameters in Fig. 3. In agreement with the above-mentioned experimental studies, the maximum of the $\varepsilon(T)$ curves shifts to higher temperatures for stronger dc fields.

With the knowledge of $\alpha(T)$ and $\beta(T)$, and with Eq. (3), the dielectric polarization can be calculated as a function of temperature and applied field (Fig. 5). Note that the strongest polarization (for a given field) has not been reached at 4.2 K, but at a higher temperature which increases with the applied field.

Together with the published value of 40 MV/m for the breakdown voltage at 4.2 K, an extrapolation of Eq. (3) to higher values of E, using the values of α and β from Fig. 3, leads to the conclusion that the maximum polarization P_{max} that can be induced in $SrTiO_3$ by application of an electric field is $P_{max} \lesssim 0.2$ C/m^2 at 4.2 K. This value lies very close to the experimentally achieved polarization in thin films of ferroelectric $[(Pb(Mg_{1/3}Nb_{2/3})O_3)_{65}(PbTiO_3)_{35}$: 0.21 C/m^2,[29] $Pb[(Fe_{0.7}Cr_{0.2}Ni_{0.1})_{0.5}Nb_{0.5}]O_3$: 0.28 C/m^2,[30]

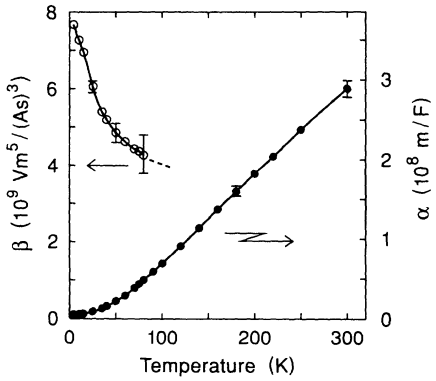

FIG. 3. Temperature dependence of the fit parameters $\alpha(T)$ and $\beta(T)$ obtained from the data in Fig. 2. Note that the low-field dielectric constant ε_l is related to α by $\varepsilon_l = (\varepsilon_0\alpha)^{-1}$. As is obvious from Fig. 2, reasonable precision for the nonlinearity parameter β can only be obtained at lower temperatures.

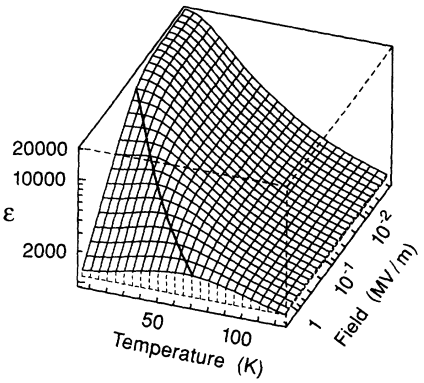

FIG. 4. The dielectric constant ε of bulk $SrTiO_3$ as a function of temperature T and field E, calculated with Eqs. (3) and (4) and using the same parameters as in Fig. 3. The bold solid line shows the field dependence of the maximum of the $\varepsilon(T)$ cuts, indicating that this maximum shifts to higher temperatures for stronger fields.

$PbTiO_3$: 0.2 C/m^2 (Ref. 31)] or "relaxor ferroelectric" $[Pb(Mg_{1/3}Nb_{2/3})O_3$: 0.15 C/m^2 (Ref. 32)] perovskites, but remains a factor of 2–4 below the values of the spontaneous polarization in single-crystal ferroelectric perovskites.[33]

IV. Pt/$SrTiO_3$:Nb DIODE *C-V* MEASUREMENTS AND DOPING DEPTH PROFILE

In the previous section, a quantitative description of the dielectric behavior of single-crystal $SrTiO_3$ was given. To be able to compare these properties with those of $SrTiO_3$ films grown on $SrTiO_3$:Nb single crystals, a characterization of these substrates is presented in this section.

As mentioned above, semiconductive properties can be induced in $SrTiO_3$ by doping, for example, with niobium. It has been shown that Nb impurities form shallow donor centers,[34] with no carrier freeze-out occurring down to 4.2

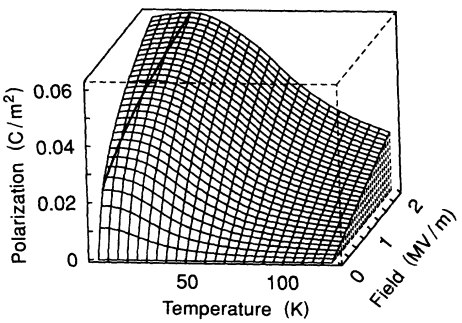

FIG. 5. Polarization of bulk $SrTiO_3$ as a function of temperature T and field E, calculated with the same parameters as in Fig. 3 and with Eq. (3). The maximum polarization for a given field is not obtained at 4.2 K, but at a temperature as indicated by the bold solid line.

K.[35] In recent work by various groups,[4,17,19,20] dopant concentrations in the range from 0.05% to 0.5% have been used. At these concentrations, $SrTiO_3$:Nb can be described as a degenerate semiconductor with a gap of about 3.2 eV.[36–38] Samples with higher concentrations show a more metallic behavior and would for that reason be preferable as electrodes; however, to minimize surface segregation[39] and interdiffusion, samples with 0.05% Nb were chosen in this work. Crystals with an even lower concentration show insulating behavior due to compensating centers such as vacancies, interstitials, dislocations, or impurities.[35]

Despite the occurrence of surface segregation in ceramics, implying that the dopant concentration is increased near the surface, it has been observed[40] that an insulating surface layer forms if $SrTiO_3$:Nb is exposed to oxygen at high temperatures (T>500 K). Likewise, the existence of an insulating layer at the interface between $SrTiO_3$:Nb and $SrTiO_3$,[4] $Ba_{1-x}K_xBiO_3$,[19] or Er-Ba-Cu-O (Ref. 20) was inferred from dielectric and transport properties of such heterostructures.

To predict the behavior of samples involving $SrTiO_3$:Nb surfaces, a better understanding of these properties is crucial. In particular, information on the depth profile of the concentration of ionized donors and on surface layers which contribute to the measured depletion layer capacitance is required. Such information can be gained from C-V measurements of metal/$SrTiO_3$:Nb contacts.

With this objective, Pt/$SrTiO_3$:Nb Schottky diodes were fabricated using a process chosen to resemble the one employed to fabricate the heterostructures studied below. ⟨100⟩-oriented surfaces of $SrTiO_3$:Nb single crystals, grown with the zone-melting technique,[14] were subjected to the same polishing, etching, and heat treatment (600 °C in 0.05 mTorr Ar:O_2=2:1) as were the substrates prior to film deposition, and then cooled to room temperature. Subsequently, platinum dots were evaporated *in situ* to serve as Schottky contacts. Several Ag contacts were diffused into the back side of the $SrTiO_3$:Nb crystal, and their Ohmic behavior was verified by measuring the two-point I-V characteristic between any two of them.

Simultaneous I-V and C-V measurements were performed on such diodes at 4.2 K. The results are shown in Figs. 6(a) and 6(b). In the forward direction (+ on the Pt electrode), the current grows by almost two orders of magnitude when the voltage is increased by 10 mV from V=746 mV (6 nA/mm^2) to V=756 mV (204 nA/mm^2), suggesting the flat-band voltage to lie within this interval.

To obtain the depth profile of the free-carrier density $n(x)$ (x being the distance from the surface) from the C-V curve, the nonlinear $P(E)$ relation [Eq. (3)] with the parameters $\alpha(T)$ and $\beta(T)$ of Fig. 3 is used. For the calculation, an iterative procedure is employed: The C-V curve resulting from a first choice of $n(x)$ is compared with the data, and the difference is used to derive a new approximation of $n(x)$. The iteration is repeated until the agreement between the calculated and the measured C-V curve is better than the experimental confidence.

Contrary to the Schottky model, where the capacitance diverges at the flat-band voltage V_{fb}, the sample in Fig. 6 has a capacitance of about 60 nF/mm^2 near $V = V_{fb}$. This disparity is modeled by assuming the existence of a capacitance in series with the depletion layer (this assumption is consistent, for example, with the presence of an insulating surface layer less than 1 nm thick of a material with ε=5).

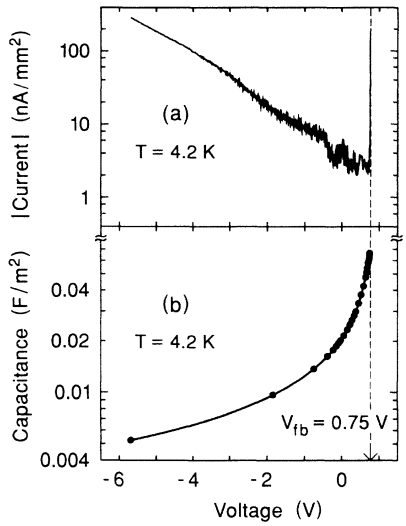

FIG. 6. (a) Current-voltage and (b) capacitance-voltage characteristics of a Pt/$SrTiO_3$:Nb-diode at 4.2 K. Solid lines represent measurements; dots depict the calculated capacitance from the carrier density profile shown in Fig. 7.

The depth profile $n(x)$ obtained from the data of Fig. 6 is shown in Fig. 7. The corresponding calculated C-V curve, indicated as dots in Fig. 6, agrees with the experimental data. Note that the values of $n(x)$ for $x < 0.5$ μm are strongly influenced by the exact value of V_{fb} and are thus of tentative nature only. This is also the case for $x > 3$ μm, because the value of n is sensitive to both C and $\partial C/\partial V$, which are both small at large voltages and thus known with less precision. In addition, cumulative errors can also influence $n(x)$ for large x, and it is therefore possible that the strong increase of $n(x)$ observed in Fig. 7 near 3 μm is partially a numerical artifact.

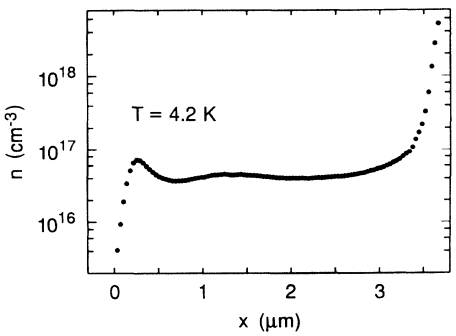

FIG. 7. Free-carrier density depth profile for a Pt/$SrTiO_3$:Nb diode calculated from the C-V data in Fig. 6. Note the large area with almost constant, but low, carrier density. See text for details.

These calculations show that in the relevant depth range (less than about 3 μm) the density of ionized Nb donors at 4.2 K lies near 4×10^{16} cm^{-3}, i.e., 200 times lower than the original doping level of 0.05 mol.% = 8×10^{18} cm^{-3}, but in agreement with the observed high surface resistivity.

Hall measurements performed on $SrTiO_3$:Nb surfaces that have not been exposed to oxygen at high temperatures[17,18] yielded values of n very close to the nominal Nb concentration. This suggests that the untreated sample, in which oxygen vacancies are charge compensated by various defects, oxidizes near the surface during exposure to oxygen at high temperatures, whereby the compensating charge traps are emptied. It is also possible that oxygen is chemisorbed at defects produced by polishing, which partially depletes the surface region, similar to what is observed in ceramics of Nb-doped $(Sr,Ca)TiO_{3-x}$.[41]

To predict the behavior of $SrTiO_3/SrTiO_3$:Nb heterostructures, the value of the free carrier concentration obtained by the above method is considered. The low carrier density leads to large depletion layer widths, and thus to low values of the capacitance measured on the metal-insulator-$SrTiO_3$:Nb diodes. It will be shown in the next section that these predictions agree with the measurements.

V. $SrTiO_3$ FILMS ON $SrTiO_3$:Nb SUBSTRATES

A. Sample preparation and analysis

Epitaxial $SrTiO_3$ films have been sputtered onto ⟨100⟩-oriented surfaces of 0.05% Nb-doped $SrTiO_3$ single crystals at 600 °C and in a 0.05 Torr $Ar:O_2 = 2:1$ sputter gas. With a rf power of 150 W and a target-substrate distance of 2.5 cm, the growth rate was 40 Å/min as determined from cross-sectional transmission electron micrographs.

Prior to deposition of the films, the substrate had been polished and etched in the same way as the bulk samples discussed in Sec. III. The surface was analyzed with a commercially available atomic force microscope (AFM) using optical beam deflection to monitor the displacement of a microfabricated Si_3N_4-type cantilever. Images of an etched and an unetched surface are shown in Fig. 8. The roughness of the etched surface was 5.5 nm (rms) as compared to the 3.9 nm (rms) of the unetched substrate. However, the latter shows individual hillocks with heights exceeding 20 nm, which are removed by etching. This explains at least in part why the capacitance of films grown on etched substrates was about 10% larger.

A magnesium top electrode (50–100 nm) was deposited *in situ* by electron beam evaporation at room temperature. Magnesium was chosen because it provides the best Ohmic contacts of all metals tested, which included gold, silver, indium, and indium-gallium, both on reduced and Nb-doped $SrTiO_3$. The Ohmic character of the Mg/$SrTiO_3$:Nb contacts indicates that the transport properties of this junction are not affected by an insulating MgO layer expected to form at the interface.

Samples were also prepared with a 40-nm-thick sputtered epitaxial $YBa_2Cu_3O_{7-x}$ top electrode. The dielectric behavior of these heterostructures could not be distinguished from that of the Mg/$SrTiO_3$/$SrTiO_3$:Nb samples, indicating the independence of these properties in the top electrode material.

The $SrTiO_3$ films grown on such substrates were analyzed using transmission electron microscopy (TEM). Standard techniques for preparing cross-sectional specimen[42] were used, and the microscopy was performed at 200 kV in a Jeol 2010. The $SrTiO_3$ films were found by electron diffraction and lattice imaging to be ⟨100⟩ oriented and grown homoepitaxially on the doped substrates.

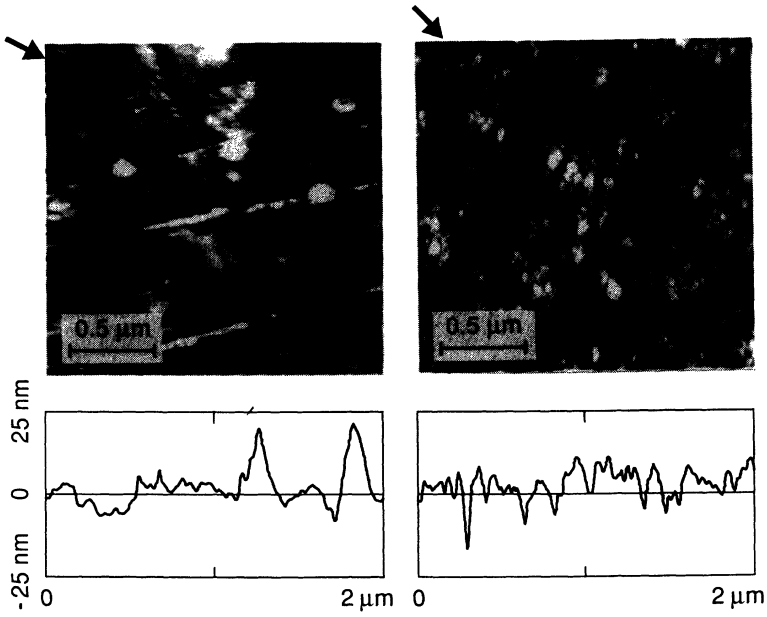

FIG. 8. Atomic force microscope image and height profile of (left) a polished and (right) a polished and etched ⟨100⟩-oriented surface of $SrTiO_3$:Nb. Etching increases the surface roughness from 3.9 nm (rms) to 5.5 nm (rms), but also removes the large individual hillocks on the unetched surface. Scratches with a typical depth of ≈10 nm incurred by polishing are visible as dark traces across the images. Arrows in the micrographs indicate the position of the cuts represented as height profiles beneath the images.

Figure 9 shows a TEM micrograph obtained of a specimen with a $Au/YBa_2Cu_3O_{7-x}$ top electrode. As seen in this figure, $SrTiO_3$ films are defective and have a larger defect density than the substrates. Due to grinding and polishing, the substrates themselves exhibit a higher dislocation density near the surface than in the typical bulk material, such as observed at a depth of > 6 μm below the surface.

The dielectric properties of $SrTiO_3$ films in such heterostructures are expected to differ from those of single-crystal samples due to surface roughness and defects. The sample capacitance will be lowered by the resulting mechanical stress and by inhomogeneities of the electric field within the film, and the breakdown strength is expected to vary from one sample to another.

B. Results of $\epsilon(T)$, $P(V)$, and $C(V)$ measurements

1. $\epsilon(T)$

Insight into the film's behavior is provided by the temperature dependence of the sample capacitance C zero field bias. The results are displayed in Fig. 10, where the temperature dependence of the quantity ε_{eff} is shown as defined by

$$\varepsilon_{\text{eff}} = \frac{1}{\varepsilon_0} \frac{d}{A} C, \tag{5}$$

where d is the film thickness and A the top electrode surface. Measurements were performed with a test signal amplitude of 50 mV and a frequency of 10 kHz. Fringe effects were neglected because of the large ratio of electrode surface area to film thickness. In general, ε_{eff} will not be equal to the film's dielectric constant due to a depletion layer in the substrate.

Two curves $\varepsilon_{\text{eff}}(T)$ are traced in Fig. 10 to demonstrate the range over which the samples' characteristics vary. Such changes of up to 20% between nominally identical specimens are attributed to variations of the properties of the substrate surface and film quality. The occurrence of a maximum of the $\varepsilon_{\text{eff}}(T)$ curves at about 30–40 K indicates that the behavior of the insulating $SrTiO_3$ is influenced by work function differences and interface trapped charges, leading to an electric field of $10^5 - 10^6$ V/m (Fig. 4).

2. $P(E)$

In order to find the maximum polarization that can be induced in $SrTiO_3$ films, the dependence of the polarization on an applied voltage was studied. For this, the current was measured and integrated while the amplitude of the applied ac voltage (1 mHz) was increased to near breakdown. No difference was visible between the curves obtained at 1 and at 10 mHz, and it is therefore assumed that these values are close to the static proper-

FIG. 9. TEM micrograph of an $Au/YBa_2Cu_3O_{7-x}/SrTiO_3/SrTiO_3$:Nb heterostructure. This bright field image shows dislocations seen as shades and dark traces coming to the surface of the $SrTiO_3$:Nb substrate in addition to the homoepitaxial $SrTiO_3$ layer with a higher dislocation density and a rather rough upper surface. Interestingly the $YBa_2Cu_3O_{7-x}$ upper surface is somewhat flatter. Also visible in this image is the top electrode of polycrystalline gold. Arrows indicate the $SrTiO_3/SrTiO_3$:Nb interface.

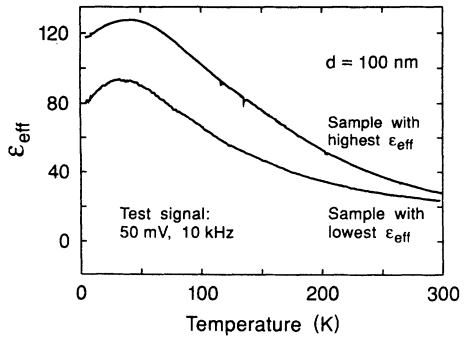

FIG. 10. Temperature dependence of the effective dielectric constant ε_{eff} defined in Eq. (5) for 100-nm-thick films. Two curves are plotted for the samples with the highest and the lowest observed values of ε_{eff} in order to indicate the variations from one sample to another.

ties. The result for a 100-nm-thick film at 4.2 K is shown in Fig. 11. A slight hysteresis is observed. Charge trapping at electrodes and interfaces is a possible explanation for this phenomenon.

Owing to trapped charges and work function differences, the film is polarized at zero applied voltage; however, this polarization cannot be obtained from our dielectric measurements. Therefore we define the quantity ΔP_i as

$$\Delta P_i = P(V_{\max}) - P(V_{\min}) , \tag{6}$$

where $V_{\max}$ and $V_{\min}$ are the extreme values of the voltage that can be applied in an experiment; i.e., they lie just below the breakdown values. Thus, ΔP_i is a measure of the maximum additional polarization that can be induced by a voltage bias.

For the sample in Fig. 11, a value of $\Delta P_i \approx 80$ mC/m^2 is found, which is about a factor of 5 below the limit extrapolated from the single-crystal properties of $SrTiO_3$ at lower fields. For this sample, the breakdown strength is 5.2 V in the forward direction, compared to less than 3.5 V for the opposite polarity. A strong dependence of these values on the sample history is observed. For example, a specimen for which the field was first swept to negative and then to positive voltages showed different breakdown characteristics than one undergoing the opposite treatment. Breakdown strengths in excess of 35 V were observed on many samples, while the values of ΔP_i did not vary much from one film to another.

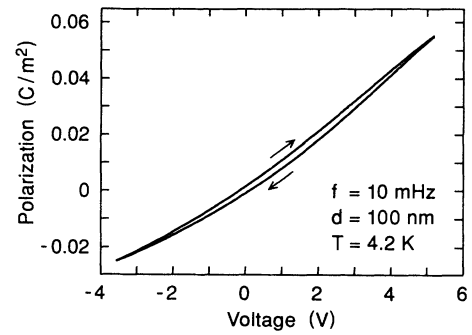

FIG. 11. Dielectric polarization versus applied voltage for a 100-nm-thick film at 4.2 K. The curve is obtained by averaging the results of several sweeps at 10 mHz, with a voltage amplitude chosen as close as possible to the breakdown values at both polarities. Arrows indicate sweep direction.

3. C(V)

With the above method to study polarization, precise results can only be acquired after repeated voltage sweeps; no information is obtained on the original state of the sample before application of the maximum voltage. Thus, capacitance-vs-voltage measurements were also performed as they do not have this serious drawback.

Figure 12 shows C-V curves for two samples with film thicknesses of 100 and 200 nm, respectively, both measured at 4.2 K. The curves were obtained by measuring the sample capacitance at 10 kHz with a test signal of 50 mV peak to peak, while the dc bias was swept to successively larger voltages. As the bias is swept from zero to positive voltage (positive polarity at the top electrode), the capacitance first goes through a maximum, then falls off sharply. Sweeping back towards negative bias, the maximum occurs at a higher voltage, the value of which depended on the maximum positive bias applied. At the same time, the value of the capacitance is strongly reduced. The effect of the negative bias is comparatively small and reversible: If the bias is being swept between given voltages, repeated cycling does not modify the shape of the traced hysteretic curve. However, every time the maximum positive field is increased, a change

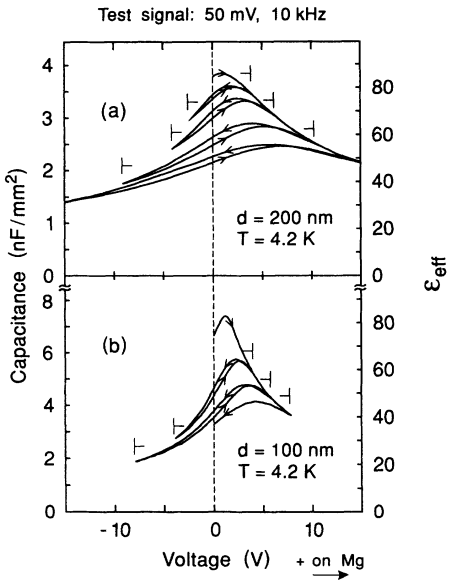

FIG. 12. Effective dielectric constant ε_{eff} defined in Eq. (5) at 4.2 K of two Mg/$SrTiO_3$/$SrTiO_3$:Nb heterostructures with $SrTiO_3$ film thicknesses of 100 and 200 nm. The bias voltage was swept to successively higher values, indicated by ⊢ and ⊣, at a rate of 0.5 V/min.

of the $C(V)$ curve's shape is observed.

After application of a positive bias, the reduced capacitance seems to correspond to a stable state of the sample at these low temperatures, with the original values being recovered only after heating the sample to temperatures higher than about 200 K. To investigate the cause of such a decrease, a constant voltage was applied to an otherwise virgin sample at various temperatures, after which the time dependence $C(t)$ of the capacitance was measured upon removal of the bias. At temperatures above 260 K, the characteristic times were shorter than the typical duration of such an experiment (2 h), and the $C(t)$ curves were fitted by the sum of two exponentials. The temperature dependence of the time constants is compatible with activation energies of 0.15 and 0.33 eV, respectively, suggesting charge trapping at the film-substrate interface as a possible cause of the lowering of the capacitance.

It is interesting to compare the values of the capacitance measured on the first sweep to positive voltages (accumulation) with the dielectric constant of bulk single-crystal $SrTiO_3$. This is done in Fig. 13, where the data of Fig. 12 (for the thin films) and of Fig. 2 (for a bulk sample) are plotted in one graph. The values of ε_{eff} are traced versus the apparent electric field E^*, defined by

$$E^* = \frac{V}{d}, \tag{7}$$

where V is the applied voltage, and d is the thickness of the thin film or the bulk sample. Note that for thin film samples, E^* is not necessarily equal to the field across the film, because the voltage drop across the depletion layer in the substrate may persist to positive voltages (forward bias) due to trapped charges. For the largest positive voltages, where the depletion layer is expected to vanish, there is reasonable agreement between data for the films and values extrapolated from the bulk. The difference lies well within a factor of 2–3, and is attributed to film imperfections. There is a strong discrepancy between bulk properties and film data for lower fields, however, which will be explained in the following.

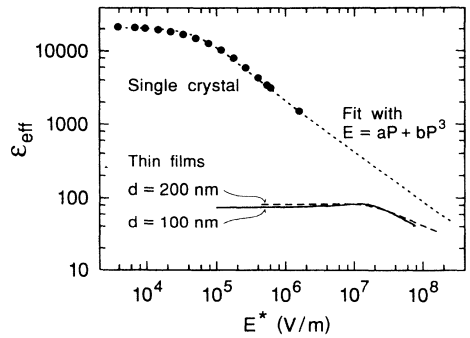

FIG. 13. Comparison of the dielectric constant of single-crystal $SrTiO_3$ (points are data from Fig. 2) and the effective dielectric constant of $SrTiO_3$ thin films (solid and dashed curves, data from Fig. 12) for film thicknesses of 100 and 200 nm, respectively. E^* is the apparent electric field defined in Eq. (7). Single-crystal data is extrapolated using Eqs. (3) and (4).

C. Model and calculations

The data presented above show strong qualitative and quantitative deviations from the single-crystal properties discussed in Sec. III. Nevertheless, considering the results obtained for $SrTiO_3$ and $SrTiO_3$:Nb, a simple model can be built to explain most of the characteristics of the presented thin film data, such as (i) the occurrence of a maximum near 30 K in the $C(T)$ curves, (ii) the relatively small value of the capacitance of the sample at zero external bias, (iii) the occurrence of a maximum of the $C(V)$ curves at a positive voltage, (iv) the shift of this maximum to higher voltages after application of a positive bias, and (v) the lowering of the capacitance after positive biasing.

The model is based on the following assumptions: (i) the relation $E = \alpha P + \beta P^3$ holds for both the film and the substrate, (ii) the depletion approximation is valid in the substrate, (iii) charge trapping occurs at the film-substrate interface when the semiconducting substrate is biased into accumulation, and (iv) some charge Q_{it} is already trapped at this interface at the beginning of the experiment.

Calculation entails the numerical integration of the one-dimensional Maxwell equation $\partial D(x)/\partial x = \rho(x)$, where $\rho(x)$ is the charge density at a depth x from the top electrode and $D(x)$ the electric displacement. Using the surface charge on the metal electrode as a boundary condition $D(x{=}0)$ and calculating the voltage across the sample by integrating $V{=}\int E(x)\,dx$ with $\varepsilon_0 E{=}D{-}P$, the capacitance of the $Mg/SrTiO_3/SrTiO_3$:Nb heterostructure is found as a function of the bias field and the sample history (which determines the density of trapped charges). The results for several sweeps with repeatedly increased amplitude at 4.2 K are shown in Fig. 14. The calculations are based on the parameters α and β as obtained in Sec. III and on the carrier density of the $SrTiO_3$:Nb substrate as calculated in Sec. IV. With this, the only free parameter is the original interface-trapped charge Q_{it}. In order to obtain reasonable qualitative agreement with experiment, this value is set to $Q_{\text{it}} = 0.143\ \text{C/m}^2 = 8.9 \times 10^{13}\ \text{cm}^{-2}$, lower than the typical value observed on clean silicon surfaces (Ref. 43, p. 380). This interface charge density leads to an internal field of 7.1×10^5 V/m across the film at zero bias, in good agreement with the values found in Sec. V B 1 [10^5–10^6 V/m, as derived from the maximum in the $\varepsilon(T)$ curves].

Owing to the surface charge Q_{it}, the top region of the substrate is depleted for $V = 0$ (situation 1 in Fig. 14). A sketch of the corresponding band diagram is shown in Fig. 15. The capacitance of the sample is the result of the series connection of the film and the depletion layer, with the field across the film being nonzero. Both effects reduce the measured capacitance compared to single-crystal capacitors.

As the applied voltage is swept to positive values, the depletion layer width decreases, tending to increase the capacitance of the sample, whereas at the same time the field across the film grows, reducing its capacitance due to the nonlinear *P(E)* relation. Both effects compete in

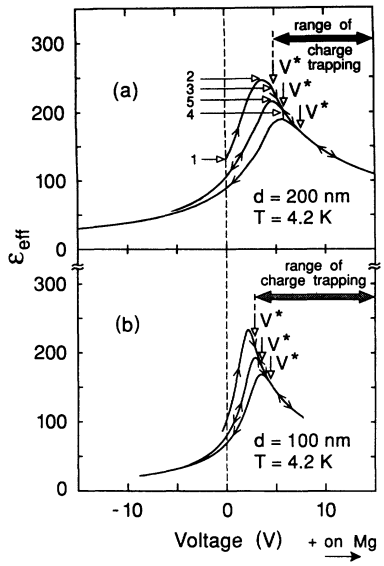

FIG. 14. Calculated dependence of ε_{eff} of $Mg/SrTiO_3/SrTiO_3$:Nb heterostructures on the applied voltage for consecutive sweeps. At each sweep, the voltage V^*, at which the depletion layer vanishes, increases. Charge trapping occurs above this voltage. Labels (1) – (5) correspond to the band diagrams in Fig. 15.

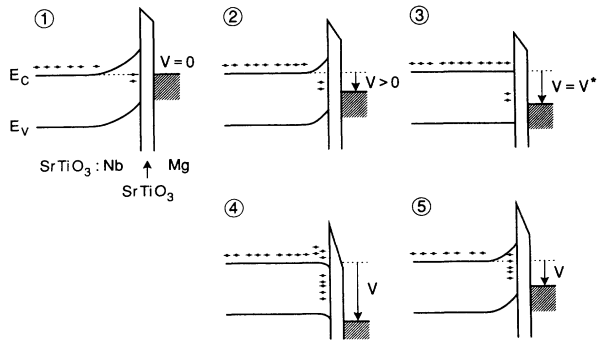

FIG. 15. Sketches of the band diagrams corresponding to the situations labeled in Fig. 14 (electrons are represented as •): (1) depletion at zero applied voltage due to trapped charges, (2) maximum of the capacitance in moderate depletion, (3) vanishing of the depletion layer at V^*, (4) charge trapping in the accumulation, and (5) additional trapped charges leading to a smaller maximum at a higher voltage.

such a manner that there exists a voltage at which the capacitance goes through a maximum (situation 2). This voltage obviously depends on the amount of charge originally trapped at the interface.

An even stronger forward bias ultimately drives the substrate into accumulation at a voltage V^* (situation 3). At higher bias, the measured capacitance of the sample therefore corresponds to the dielectric properties of the $SrTiO_3$ film and shows $C \propto V^{-2/3}$ behavior (situation 4).

To explain the shift of the maximum in the $C(V)$ curves, it is now assumed that a large proportion (0.8) of the accumulated charge remains trapped at the interface. Therefore, when the bias is reduced again, the situation is changed with respect to the first sweep in the positive direction, with a lower maximum in the $C(V)$ curve occurring at a higher voltage (situation 5).

Qualitatively, this model reproduces the main features of the experimental results. However, the calculated values are about a factor of 3–4 higher than the measurements. This discrepancy and the one observed for the ΔP_i values are discussed in the following.

It is recalled that all calculations of interest here are based on an extrapolation of $\varepsilon(E)$ from measurements at fields lower than 2×10^6 V/m (Fig. 2) where fifth- and higher-order terms in the $E(P)$ development [Eq. (3)] cannot be obtained. Such additional terms further reduce ε at higher fields. Inhomogeneities of the electric field in the film caused by the surface roughness of the substrate and by defects will lead to parts of the film material with a lowered ε due to the increased local field; obviously, these inhomogeneities will also reduce the breakdown strength. In addition, mechanical stress leads to a further decrease of the polarizability of $SrTiO_3$.[3] It is assumed that these effects explain the differences between the measured values and those calculated from the simple model.

VI. CONCLUSIONS

A detailed study of the dielectric behavior of $SrTiO_3$ thin films has been presented together with a quantitative description of dielectric and transport properties of single-crystal $SrTiO_3$ and $SrTiO_3$:Nb. The dielectric characteristics of $SrTiO_3$ films in $Mg/SrTiO_3/SrTiO_3$:Nb heterostructures can be understood qualitatively from bulk properties of $SrTiO_3$ and $SrTiO_3$:Nb. The field dependence of the dielectric constant of $SrTiO_3$ resulting from the nonlinear relation between an applied field E and the polarization P, given by $E = \alpha P + \beta P^3$, needs to be taken into account together with the $SrTiO_3$:Nb substrate's low carrier density observed in a surface region of a few micrometers. The observed shift of the maximum of the $C(V)$ curves is attributed to strong charge trapping at the film-substrate interface.

Results of numerical calculations based on these assumptions agree qualitatively with the observed C-V curves and the $\varepsilon(T)$ dependence of the $Mg/\text{-}SrTiO_3/SrTiO_3$:Nb heterostructures. The quantitative agreement lies within a factor of 4.

The maximum dielectric polarization of $Mg/\text{-}SrTiO_3/SrTiO_3$:Nb heterostructures depends both on the polarizability and the breakdown strength of the $SrTiO_3$ films. The value of 80 mC/m^2 observed in the present study lies about a factor of 5 below the value extrapolated from the behavior of single crystals.

Mechanical stress as well as inhomogeneities of the electric field resulting from surface roughness and defects are suggested as reasons for the differences between calculated and measured values.

ACKNOWLEDGMENTS

It is our pleasure to acknowledge the fruitful collaboration with J. G. Bednorz, A. Châtelain, T. Frey, D. G. Schlom, J. Ströbel, and K. Wachtmann.

* Author to whom correspondence should be sent. Electronic address: hmc@zurich.ibm.com

[1] M.E. Lines and A.M. Glass, *Principles and Applications of Ferroelectrics and Related Materials* (Clarendon Press, Oxford, 1977).
[2] J.C. Burfoot and G.W. Taylor, *Polar Dielectrics and their Applications* (MacMillan, London, 1979).
[3] K.A. Müller and H. Burkard, Phys. Rev. B **19**, 3593 (1979).
[4] J. Mannhart, D.G. Schlom, J.G. Bednorz, and K.A. Müller, Z. Phys. B **83**, 307 (1991).
[5] J. Mannhart, D.G. Schlom, J.G. Bednorz, and K.A. Müller, Phys. Rev. Lett. **67**, 2099 (1991).
[6] A. Walkenhorst, C. Doughty, X.X. Xi, S.N. Mao, Q. Li, T. Venkatesan, and R. Ramesh, Appl. Phys. Lett. **64**, 1744 (1992).
[7] K. Sakuta, T. Awaji, K. Matsui, T. Hirano, T. Fujii, and T. Kobayashi, Jpn. J. Appl. Phys. **31**, L1411 (1992).
[8] R.B. Laibowitz, J.Z. Sun, V. Foglietti, W.J. Gallagher, and R.H. Koch, Appl. Phys. Lett. **64**, 247 (1994).
[9] S.H. Nam, N.H. Cho, and H.-G. Kim, J. Phys. D **25**, 727 (1992).
[10] S.H. Nam and H.-G. Kim, J. Appl. Phys. **72**, 2895 (1992).
[11] P.C. Joshi and S.B. Krupanidhi, Appl. Phys. Lett. **61**, 1525 (1992).
[12] D. Roy, C.J. Peng, and S.B. Krupanidhi, Appl. Phys. Lett. **60**, 2478 (1992).
[13] T. Kuroiwa, T. Honda, H. Watarai, and K. Sato, Jpn. J. Appl. Phys. **31**, 3025 (1992).
[14] J.G. Bednorz and K.A. Müller, Phys. Rev. Lett. **52**, 2289 (1984).
[15] J.F. Schooley, W.R. Hosler, and M.L. Cohen, Phys. Rev. Lett. **12**, 474 (1964).
[16] G. Binnig, A. Baratoff, H.E. Hoenig, and J.G. Bednorz, Phys. Rev. Lett. **45**, 1352 (1980).
[17] H. Takauchi, A. Yoshida, H. Tamura, and S. Hasuo, Appl. Phys. Lett. **61**, 1462 (1992).
[18] H. Suzuki, M. Iyori, T. Yamamoto, S. Suzuki, K. Takahashi, T. Usuki, and Y. Yoshisato, Jpn. J. Appl. Phys. **31**, 2716 (1992).
[19] H. Suzuki, T. Yamamoto, S. Suzuki, M. Iyori, K. Takahashi, T. Usuki, Y. Yoshisato, and S. Nakano, Jpn. J. Appl. Phys. **32**, 783 (1993).
[20] H. Hasegawa, T. Fukazawa, and T. Aida, Jpn. J. Appl. Phys. **28**, L2210 (1989).
[21] K. Abe and S. Komatsu, Jpn. J. Appl. Phys. **32**, L1157 (1993).
[22] R.C. Neville, B. Hoeneisen, and C.A. Maed, J. Appl. Phys. **43**, 2124 (1972).
[23] H.H. Barrett, J. Appl. Phys. **35**, 1420 (1964).
[24] E. Hegenbarth, Phys. Status Solidi **6**, 333 (1964).
[25] D. Itschner, Ph.D. thesis, Swiss Federal Institute of Technology, Zurich, Switzerland, 1965.
[26] M.A. Saifi and L.E. Cross, Phys. Rev. B **2**, 677 (1970).
[27] J.D. Jackson, *Classical Electrodynamics* (John Wiley, New York, 1975).
[28] G.P. Agrawald, *Nonlinear Fiber Optics* (Academic Press, San Diego, 1989).
[29] K.R. Udayakumar, J. Chen, P.J. Schuele, L.E. Cross, V. Kumar, and S.B. Krupanidhi, Appl. Phys. Lett. **60**, 1187 (1992).
[30] C.V.R. Vasant Kumar, M. Sayer, and R. Pascual, Appl. Phys. Lett. **60**, 2080 (1992).
[31] H. Tabata, O. Murata, T. Kawai, S. Kawai, and M. Okuyama, Jpn. J. Appl. Phys. **31**, 2968 (1992).
[32] C.V.R. Vasant Kumar, M. Sayer, and R. Pascual, Appl. Phys. Lett. **60**, 2207 (1992).
[33] S.C. Abrahams and E.T. Keve, Ferroelectrics **2**, 129 (1971).
[34] O.N. Tufte and P.W. Chapman, Phys. Rev. **155**, 796 (1967).
[35] H.P.R. Frederikse, W.R. Thurber, and W.R. Hosler, Phys. Rev. **134**, A442 (1964).
[36] H.W. Gandy, Phys. Rev. **113**, 795 (1959).
[37] K.W. Blazey, Phys. Rev. Lett. **27**, 146 (1971).
[38] G. Campet, S.Z. Wen, C. Puprichitkun, J.P. Manaud, and J. Claverie, Phys. Status Solidi A **103**, 175 (1987).
[39] S.B. Desu and D.A. Payne, J. Am. Ceram. Soc. **73**, 3398 (1990).
[40] I. Burn and S. Neirman, J. Mater. Sci. **17**, 3510 (1982).
[41] Y. Nakano, M. Watanabe, and T. Takahashi, J. Appl. Phys. **70**, 1539 (1991).
[42] S.B. Newcomb, C.B. Boothroyd, and W.M. Stobbs, J. Microsc. (Oxford) **140**, 195 (1985).
[43] S.M. Sze, *Physics of Semiconductor Devices*, 2nd ed. (John Wiley, New York, 1981).

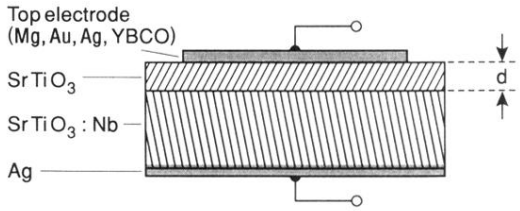

FIG. 1. Sample structure to study the dielectric properties of $SrTiO_3$ films. Mg, Au, Ag, and $YBa_2Cu_3O_{7-x}$, have been used as top electrode. The typical thickness d of the $SrTiO_3$ film is between 30 and 200 nm.

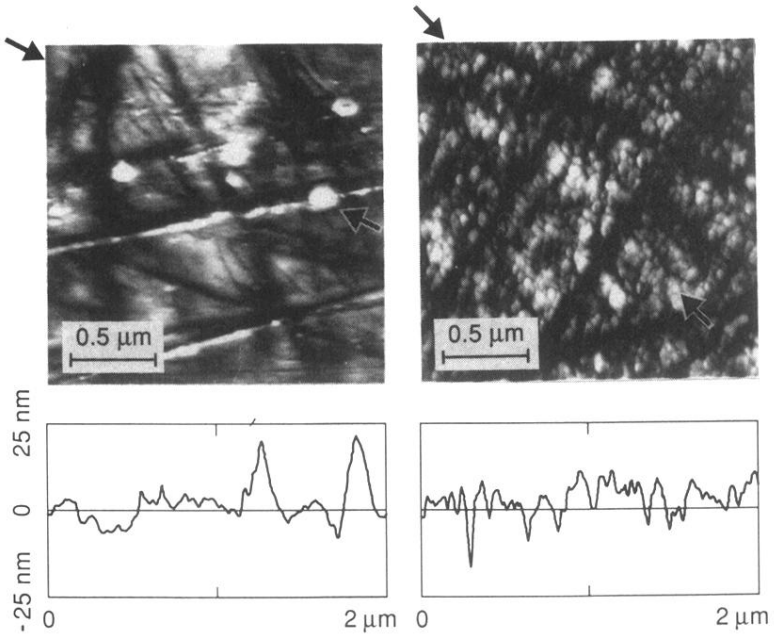

FIG. 8. Atomic force microscope image and height profile of (left) a polished and (right) a polished and etched ⟨100⟩-oriented surface of $SrTiO_3$:Nb. Etching increases the surface roughness from 3.9 nm (rms) to 5.5 nm (rms), but also removes the large individual hillocks on the unetched surface. Scratches with a typical depth of $\approx$10 nm incurred by polishing are visible as dark traces across the images. Arrows in the micrographs indicate the position of the cuts represented as height profiles beneath the images.

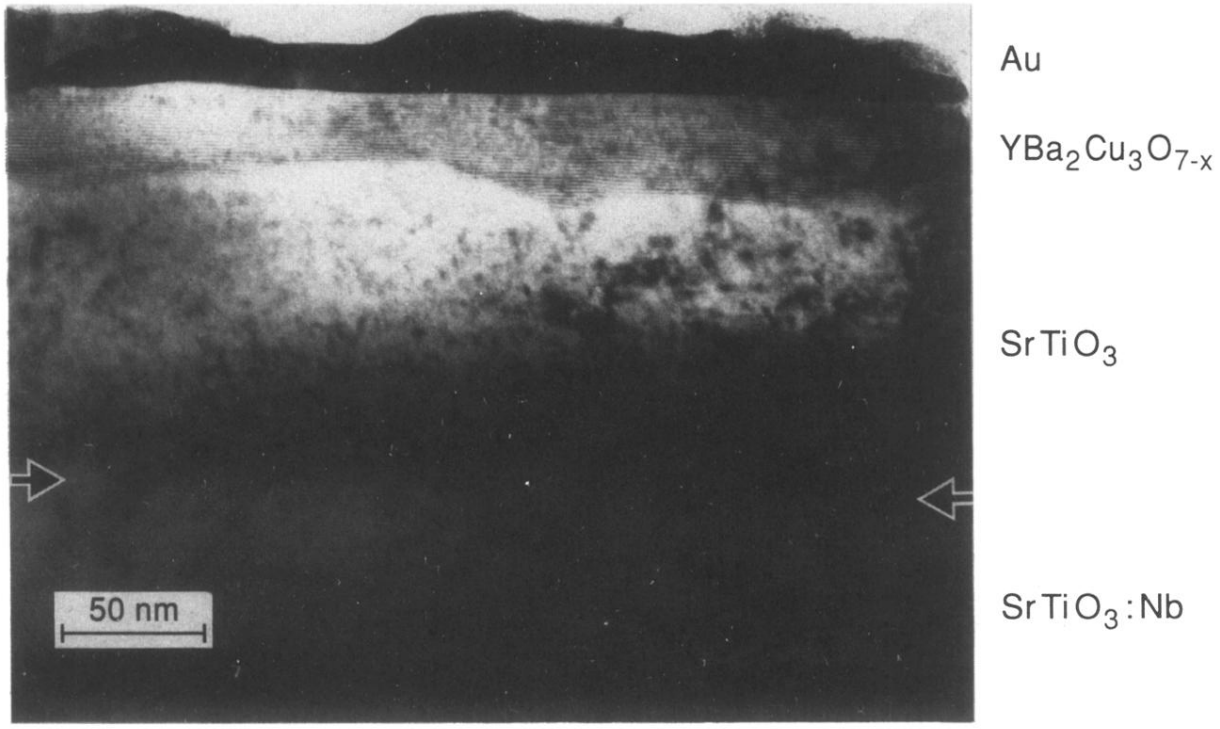

FIG. 9. TEM micrograph of an $Au/YBa_2Cu_3O_{7-x}/SrTiO_3/SrTiO_3$:Nb heterostructure. This bright field image shows dislocations seen as shades and dark traces coming to the surface of the $SrTiO_3$:Nb substrate in addition to the homoepitaxial $SrTiO_3$ layer with a higher dislocation density and a rather rough upper surface. Interestingly the $YBa_2Cu_3O_{7-x}$ upper surface is somewhat flatter. Also visible in this image is the top electrode of polycrystalline gold. Arrows indicate the $SrTiO_3/SrTiO_3$:Nb interface.